The generality of surface vanadium oxide phases in mixed oxide catalysts

Israel E. Wachs *

Operando Molecular Spectroscopy & Catalysis Laboratory, Department of Chemical Engineering, Lehigh University, Bethlehem, PA 18015, USA

ARTICLE INFO

ABSTRACT

The nature of VO_x sites in mixed oxides of supported VO_x (on both pure oxide and mixed oxide supports), molecular sieves, zeolites, clays, hydrotalcites, stochiometric bulk oxides and bulk solid solutions were investigated. For supported metal oxides, zeolites and molecular sieves, the VO_x species are exclusively present as surface VO_x phases below monolayer coverage or the maximum dispersion limits. For layered clays and hydrotalcites, the VO_x is present in the hydroxide layers at modest temperatures and react with the clays and hydrotalcites at higher temperatures ($>350\,^\circ$C) when their layered structures decompose. Surface VO_x species are always also present for bulk oxides and bulk solid solutions. The rapid diffusion kinetics of VO_x, due to its low Tammann temperature, coupled with the lower surface free-energy of vanadium oxide are responsible for the universal presence of surface VO_x sites on all mixed oxide materials. Furthermore, surface reactivity studies demonstrate that the surface VO_x sites are the catalytic active sites for all V-containing mixed oxide catalytic materials.

© 2010 Elsevier B.V. All rights reserved.

1. Introduction

The class of mixed metal oxide catalytic materials consists of many different metal oxide arrangements as depicted in Fig. 1. Supported metal oxides possess two-dimensional surface metal oxide phases on a high surface area supports such as pure oxides, mixed oxides, zeolites or molecular sieves) [1–11]. Layered clays and hydrotalcites allow for intercalation of metal oxides between the hydroxide layers [12,13]. Polyoxometalate (POM) clusters are nanometer sized mixed oxide clusters such as $XM_{12-x}V_xO_{40}$ or $X_2M_{18-x}V_xO_{62}$ where the central XO_4 unit can be PO_4, SiO_4, etc. and coordinated to exposed mono-oxo MO_6 (M = Mo, W, Cr, Nb, Ta or Re) or VO_6 units via its oxygen linkages [14,15]. Bulk mixed oxides can be present as stochiometric compounds (e.g., $FeVO_4$) [5,16] or solid solutions (e.g., $V_xTi_{1-x}O_2$) [17]. Such mixed metal oxides can occur in both isotropic (e.g., POMs and $FeVO_4$) as well as anisotropic platelet morphologies (i.e., V_2O_5 and $(VO)_2P_2O_7$).

This paper will only focus on the presence of surface VO_x phases in V-containing mixed oxide materials and the catalytic consequences of the presence of surface vanadium oxide sites in different mixed oxide catalytic materials. The V-containing mixed oxide materials are selected because of their extensive employment for catalytic as well as non-catalytic applications. The surface chemistry of the V-containing mixed oxides will be chemically probed with oxidation reactions because of the known redox nature of vanadium oxide. Model supported vanadium oxide catalysts will serve as references since they are known to possess 100% dispersed VO_x species below monolayer coverage or maximum dispersion limit. The V-containing mixed oxides will be characterized with IR and Raman vibrational spectroscopy, CH_3OH-temperature programmed surface reaction (TPSR) spectroscopy and steady-state oxidation reactions. The collective experimental information will show that surface VO_x phases are a general phenomenon in V-containing mixed oxide catalytic materials employing numerous examples from the author's research.

2. Experimental

2.1. Catalyst synthesis

2.1.1. Supported metal oxides

The supported vanadium oxide catalysts were synthesized by incipient wetness impregnation of V-isopropoxide dissolved in an isopropanol solution into high surface area oxide supports (e.g., Al_2O_3, ZrO_2, TiO_2, Nb_2O_5, SiO_2, supported TiO_2/SiO_2, silicalite molecular sieve and ZSM-5 zeolite) under a N_2 atmosphere in a

* Corresponding author. Tel.: +1 610 758 4274.
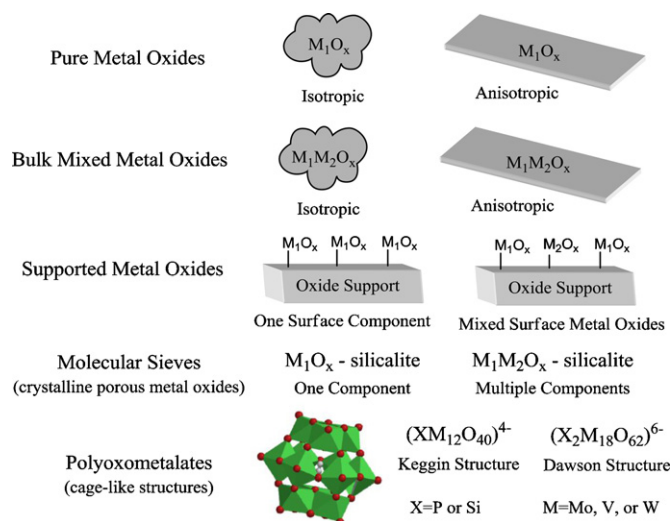*E-mail address:* iew0@lehigh.edu.

Fig. 1. Different types of metal oxide materials employed as oxidation catalysts.

glove box. The resulting samples were initially dried at room temperature and 100 °C followed by calcination in N_2 at 350 °C. After the N_2 calcination step to decompose the alkoxy ligands, the samples were subsequently calcined in air for an additional 4 h at 450 °C to form the supported vanadium oxide phases [1,2,18].

2.1.2. POMs

The $H_3PW_{12}O_{40}$ and $H_{3+x}PW_{12-x}V_xO_{40}$ ($x = 1, 2, 3$) POMs were purchased from Aldrich Chemical Co. and Nippon Inorganic Color and Chemical Co., respectively. The tungstophosphoric acid (TPA) and V-containing TPA catalysts will be denoted as TPA, TPAV1, TPAV2 and TPAV3, respectively. In addition, vanadia was also introduced onto the surface of TPA, and this catalyst is denoted as VOTPA. An aqueous solution containing an appropriate amount of VO^{2+} ions was prepared by reaction of crystalline V_2O_5 with oxalic acid at about 100 °C while maintaining the VO^{2+}/TPA molar ratio equal to 2. After complete dissolution of the V_2O_5 solid, the solution was cooled to room temperature, and the required amount of TPA was added. The excess water was then removed by evaporation at 100 °C, and the dried mass was subsequently calcined at 300 °C in air for 3 h.

2.1.3. Bulk mixed metal oxides

Bulk $FeVO_4$ was synthesized through an organic route from NH_4VO_3 (Alpha Aesar Products, 99.9%), $Fe(NO_3)_3 \cdot 9H_2O$ (Alpha Aesar Products, 99.9%) and citric acid ($HOC(COOH)(CH_2COOH)_2 \cdot H_2O$; Alfa Aesar Products, 99.9%). To 200 mL of distilled water, specific amount of ferric nitrate and citric acid were added and mixed until the complete dissolution of salts. Citric acid was added in a quantity sufficient to ensure that the molar number of equivalent anions equalled that of cations. A stoichiometric amount of NH_4VO_3 was separately added to 200 mL of distilled water and then mixed with the 200 mL of distilled water-citric acid-nitrate solution. The mixture was dried in a steam bath until a glassy textured solid was observed. The solid were further dried overnight at a temperature of 70 °C, subsequently, ground and calcined at 550 °C for 4 h in order to obtain a crystalline material [5,16,19].

2.1.4. Bulk mixed oxide solid solutions

Bulk mixed oxide solutions were prepared by coprecipitation of the two metal oxide aqueous precursors or by heating the supported V_2O_5 catalysts to elevated temperatures in which the V_2O_5 dissolved into the support lattice [16,17]. The bulk V–Nb–O mixed

oxides were prepared from ammonium vanadate (NH_4VO_3) (Alfa-AESAR, 99.93% purity) and niobium oxalate ($Nb(HC_2O_4)_5$) (CBMM, 99.5% purity). The bulk V–Nb–O mixed oxides were prepared by mixing the corresponding aqueous solutions of the starting precursors. The aqueous mixture was subsequently evaporated to dryness by stirring and heating at 150 °C. The dry precursor was subsequently calcined in air for 2 h at 600 °C to form the bulk V–Nb–O mixed oxide catalysts.

2.2. Raman spectroscopy

The in situ Raman spectra of the mixed metal oxides were collected with a Horiba-Jobin Yvon LabRam-HR spectrometer equipped with a confocal microscope, 2400/900 grooves/mm gratings, and a notch filter. The visible laser excitation at 532 nm (visible/green) was supplied by a Yag doubled diode pumped laser (20 mW). The scattered photons were directed and focused onto a single-stage monochromator and measured with a UV-sensitive LN2-cooled CCD detector (Horiba-Jobin Yvon CCD-3000 V). The powdered samples, ~5–10 mg, were loosely spread onto a small ceramic boat inside the environmental cell (Linkam T-1500) and maintained below the confocal microscope. Dehydration of the catalyst samples was carried out by heating the environmental cell to different temperatures under O_2/He or CH_3OH/O_2/He flow (30 mL/min). After the desired treatment temperature was reached, the samples were dehydrated for 30 min before the Raman spectrum was recorded [18].

2.3. IR spectroscopy

The in situ IR vibrational measurements were performed with a Fourier transform infrared spectrometer (IlluminatIR II, Smith Detection) attachment that was mounted on the Horiba-Jobin Yvon LabRam-HR spectrometer equipped with mercury telluride (HgTe) and cadmium telluride (CdTe) photoconductive detectors (MCT) and cooled using liquid nitrogen. The reflectance FT-IR spectra were collected in the total reflection mode employing 0.3 s/scan with a resolution of ~4 cm^{-1} and 1000 scans for the steady-state mode and 200 scans for temperature programmed mode.

2.4. CH_3OH-TPSR spectroscopy

The CH_3OH-TPSR spectroscopy measurements were performed on an Altamira (AMI-200) system equipped with an online quadrupole mass spectrometer (Dycor Dymaxion DME200MS). About 200 mg of sample was typically loaded into a U-shaped quartz tube and initially treated at 250 °C (ultra zero grade O_2/He, 30 mL/min) for ~1 h to remove any combustible impurities that may be present. To ensure that the catalysts remain in a fully oxidized state, the pretreated samples were first cooled in flowing air to 110 °C and then the gas stream was switched to an ultra-high-purity He flow with further cooling to 100 °C. After flushing with continuously flowing He for another 1 h at 100 °C to remove any physically adsorbed oxygen or potential background gases, a CH_3OH/He gas mixture (2000 ppm methanol) feed was introduced at 30 mL/min for CH_3OH chemisoprtion and maintained for ~40 min. Previous work demonstrated that the adsorption temperature of 100 °C almost completely minimizes the presence of physically adsorbed methanol on the catalyst samples since the physically adsorbed CH_3OH desorbs below this temperature [18]. After methanol adsorption, the mixed metal oxide catalysts were again purged at 100 °C with an ultra-high-purity (UHP) He flow for an additional 1 h to remove any residual physically adsorbed methanol. The CH_3OH-TPSR spectroscopy experiment was then performed with a heating rate of 10 °C/min in the flowing UHP He, and desorption products were monitored with the online mass

spectrometer. The m/e values used to detect the different desorption products were 31 (CH_3OH), 30 (H_2CO), 45 (CH_3OCH_3-DME), 76 (($CH_3O)_2CH_2$-DMM), 44 (CO_2), and 28 (CO). For desorbing products that gave rise to several fragments in MS, additional m/e values were also collected to confirm the identity of the desorbing products (e.g., $m/e = 45$ for $CH_3OCH_2^+$ and $m/e = 15$ for the associated CH_3^+ cracking fragment). The number of exposed redox and acid sites per gram (Ns) of each catalyst was determined from the TPSR spectra. The area under the curve for the formaldehyde peak was integrated to determine the number of redox sites, and the area under the curve for the dimethyl ether peak was integrated to determine the number of acid sites. The MS signals for HCHO and DME were calibrated against quantitative thermogravimetric analysis (TGA) measurements with exclusive redox and acid catalysts, respectively [18,20].

2.5. CH₃OH oxidation/dehydration

Steady-state methanol oxidation/dehydration was performed in an isothermal fixed-bed differential reactor, ∼10% methanol conversion, at atmospheric pressure. In a typical experiment about 30 mg of catalysts was held between two glass wool beds and pretreated under O_2/He flow at 250 °C for 30 min before passing the gaseous reactants at the desired reaction temperature. The volume composition of the gaseous reactant feed was 6% CH_3OH, 13% O_2, and balance He, with a total flow rate of ∼100 mL/min. The methanol conversion and reaction products were analyzed using an online gas chromatograph (HP 5890 series II) equipped with TCD and FID detectors. A Carboxene-1000-packed column and a CP-sil 5CB capillary column were used in parallel for TCD and FID, respectively. The catalytic turnover frequencies (TOFs) for methanol oxidation to redox products (HCHO, methyl formate (MF: CH_3OOCH), and DMM) and methanol dehydration to DME were determined by normalizing the steady-state reaction rates per gram by the number of redox and acid sites per gram of catalyst, respectively, which were determined from the CH_3OH-TPSR spectra described above [1,2,18].

2.6. Propane oxidation

Propane oxidation was carried out in an isothermal fixed-bed differential reactor (Pyrex tubing, 1/4 in. o.d. and 1 ft long) using 30–100 mg of catalyst at atmospheric pressure with reaction temperatures varying from 250 to 550 °C. Propane conversions were maintained below 6%. The reactant gas mixture of C_3H_8/O_2/He has a molar ratio of 5/40/55 with a flow rate of 50 mL/min. The reactor effluent was analyzed by an online Hewlett-Packard Gas Chromatograph 6890 Series equipped with both TCD and FID detectors. A Carboxene-1000 packed column and a Supelco capillary column (PQ1334-04) were employed in parallel for the TCD and FID, respectively. The samples were pretreated in a flowing O_2/He gas mixture at 400 °C for 0.5 h before each run. The specific catalytic activity values, turnover frequency (TOF), is defined as the number of propane molecules converted per surface V atom per second). The number of exposed surface VO_x sites for the mixed V_2O_5–Nb_2O_5 oxides was estimated by comparing the propane ODH activity of supported V_2O_5/Nb_2O_5 catalysts, containing 100% of the vanadium oxide on the surface, with the activity of the V_2O_5–Nb_2O_5 catalyst.

3. Results and discussion

3.1. Supported metal oxides

3.1.1. Pure oxide supports

Supported vanadium oxide phases on conventional high surface area oxide supports (e.g., SiO_2, Al_2O_3, TiO_2, ZrO_2, CeO_2, Nb_2O_5
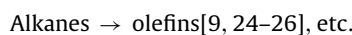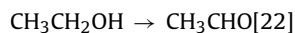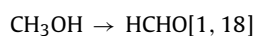
Table 1
Methanol oxidation over supported vanadia at monolayer surface coverage catalysts at 230 °C (6% CH_3OH, 13% O_2, 81% He; ∼100 mL/min).
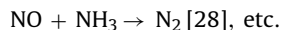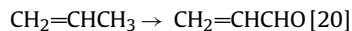
Catalyst	TOF_{redox} (s^{-1})	Selectivity$_{redox}$ (%)
V_2O_5/CeO_2	1.0×10^0	100
V_2O_5/ZrO_2	1.7×10^{-1}	99
V_2O_5/TiO_2	1.1×10^{-1}	100
V_2O_5/Nb_2O_5	8.5×10^{-2}	98
V_2O_5/Ta_2O_5	7.6×10^{-2}	100
V_2O_5/Al_2O_3	6.8×10^{-3}	50
V_2O_5/SiO_2	2.0×10^{-3}	97

and Ta_2O_5) have been extensively investigated over the past three decades and are formed when vanadium oxide precursors or even bulk V_2O_5, due to its low Tammann temperature of ∼200 °C, are deposited on high surface area oxide materials [1–4]. Only isolated, mono-oxo surface VO_4 species are present for supported V_2O_5/SiO_2 catalysts under dehydrated conditions and below the maximum dispersion limit [5–8]. Isolated, mono-oxo surface VO_4 species are also almost exclusively present at low surface coverage (<2 V/nm^2) on oxide supports [9]. At higher surface coverage, and especially as monolayer cover is approached, polymeric surface $(VO_4)_n$ species become the predominant species on oxide supports [9,10]. Supported vanadium oxide phases have also been successfully synthesized on some less traditional oxide supports such as Fe_2O_3, Cr_2O_3, NiO, MnO, Co_3O_4 and Ta_2O_5 [4,21].

The specific catalytic reaction rates (TOF: turnover frequency is defined as the number of molecules reacting per surface VO_4 site per second determined at low reactant conversions of ∼10%) have been found to be essentially independent or only weakly dependent of the surface VO_4 coverage on oxide supports for two e$^-$ reactions:

$$CH_3OH \rightarrow HCHO [1, 18]$$

$$CH_3CH_2OH \rightarrow CH_3CHO [22]$$

$$SO_2 \rightarrow SO_3 [23]$$

$$Alkanes \rightarrow olefins [9, 24–26], etc.$$

For catalytic reaction involving more than 2e$^-$, which involve the participation of more than one O atom, the TOF increases with surface coverage VO_4 coverage because multiple surface VO_4 sites need to be involved:

$$n–C_4H_{10} \rightarrow maleic\ anhydride\ [27]$$

$$CH_2=CHCH_3 \rightarrow CH_2=CHCHO\ [20]$$

$$NO + NH_3 \rightarrow N_2\ [28], etc.$$

For all oxidation reactions over supported vanadium oxide catalysts, however, the TOF values vary dramatically as a function of the specific oxide support by as much as a factor of 10^3 for many oxidation reactions [1,9,23–28] depending on the properties of the underlying oxide support. This general trend of the effect of the underlying support on the TOF values for oxidation reactions is shown below for methanol oxidation over supported vanadium oxide catalysts in Table 1. The origin of this pronounced support effect is not completely understood and is still being extensively discussed in the literature [18,29,30].

3.1.2. Model mixed oxide supports

Mixed oxide supports consist of two or more oxides intimately mixed in the bulk and the surface. Model mixed oxide supports were prepared by depositing a metal oxide on a high surface

Table 2
Activity and product selectivity of V_2O_5/SiO_2, $V_2O_5/TiO_2/SiO_2$, and V_2O_5/TiO_2 catalysts for methanol oxidation at 270 °C (6% CH_3OH, 13% O_2, 81% He; ~100 mL/min).

Catalyst	TOF (10^{-3}/s)	Selectivity (%)			
		HCHO	HCOOCH₃	DMM	DME
1% V_2O_5/SiO_2[a]	2	–	–	–	–
1% V_2O_5/1% TiO_2/SiO_2[a]	10	–	–	–	–
1% V_2O_5/5% TiO_2/SiO_2	52	82	15	3	0
1% V_2O_5/8% TiO_2/SiO_2	57	85	5	6	4
1% V_2O_5/12% TiO_2/SiO_2	72	85	5	6	4
1% V_2O_5/30% TiO_2/SiO_2	140	89	1	7	3
1% V_2O_5/50% TiO_2	420	87	7	4	3
1% V_2O_5/TiO_2	750	93	5	2	0

[a] Methanol conversion is too low to accurately determine selectivity.

area oxide support (e.g., TiO_2/SiO_2, ZrO_2/SiO_2, Al_2O_3/SiO_2, etc.) followed by calcination to form the supported metal oxide phase (e.g., TiO_2, ZrO_2, Al_2O_3, etc.). The synthesized model mixed oxide supports allow for control of the composition and structure of the mixed oxide surface. At low surface coverage, the impregnated oxide is typically present as a surface oxide overlayer and can form oxide nanoparticles at high surface coverage [31–35]. Such model mixed oxide supports can then be employed as oxide supports to for supported vanadium oxide catalysts [31–35]. For the multilayered supported $V_2O_5/TiO_2/SiO_2$ catalyst system [34–36], characterization studies demonstrated that the surface VO_4 species preferentially anchor to the surface TiO_x sites because of the higher surface free-energy of the exposed TiO_x sites than the SiO_2 support [37]. The formation of bridging V–O–Ti bonds has a dramatic effect on the TOF value of the isolated supported VO_4 species as tabulated in Table 2.

This enhancement is related to the greater reactivity of surface VO_4 sites coordinated to TiO_x sites than SiO_x sites [34–36]. The deposited TiO_2 phase is 100% dispersed as surface TiO_x species up to 12% TiO_2/SiO_2 and is present as 3–9 nm crystalline TiO_2 (anatase) rafts at higher surface coverage [32,34–36]. The Si-free supported 1% V_2O_5/TiO_2 catalyst contains ~25 nm TiO_2 crystalline particles (mainly the anatase phase). These catalytic results demonstrate that for redox surface VO_4 sites the TOF values increase with the domain size of the TiO_2 substrate in the ~0.4–25 nm range. The increased redox activity of the surface VO_4 sites with increasing TiO_2 loading also improves the HCHO selectivity by suppressing the competitive MF formation on the supported TiO_2 sites [32]. These model studies with mixed oxide supports further demonstrate the sensitivity of redox surface VO_4 sites to the nature of the underlying oxide support ligands and that surface vanadia phases also readily form on mixed oxide supports.

3.1.3. Molecular sieve and zeolite supports

The molecular sieve V–silicalite exclusively possesses isolated VO_4 sites [38]. To examine the influence of the oxide support long-range environment, the reactivity and selectivity of crystalline, nanoporous V–silicate were compared with that of amorphous mesoporous supported V_2O_5/SiO_2 which also contains isolated VO_4 sites. Raman and solid-state ^{51}V NMR analyses confirmed that both catalyst systems indeed contained isolated VO_4 units under dehydrated conditions and exhibit V=O vibrations at ~1035 cm^{-1} [38]. The reactivity and product selectivity of the two types of SiO_2-containing vanadia catalysts are listed in Table 3 and are essentially indistinguishable. The identical TOF and product selectivity for the amorphous supported V_2O_5/SiO_2 and crystalline V–silicalite catalysts reveal that the long-range order and nano- or mesoporosity of the underlying oxide support do not affect the TOF and selectivity when the same support ligands are present (in this case V–O–Si bonds).

Table 3
Activity and product selectivity for methanol oxidation at 380 °C over supported 1% V_2O_5/SiO_2 (amorphous and mesoporous) and V–silicalite molecular sieve with ~1% V_2O_5 (crystalline and nanoporous) at 380 °C (6% CH_3OH, 13% O_2, 81% He; ~100 mL/min).

Catalyst	TOF (10^{-3}/s)	Selectivity			
		HCHO	HCOOCH₃	CO	CO₂
Supported 1% V_2O_5/SiO_2	43	84.6	2.5	12.9	0
V–Silicalite	53	87.0	0.0	12.3	0.7

Impregnation of vanadium oxide precursors into ZSM-5 zeolites, that are subsequently calcined, also results in isolated surface VO_4 species that exhibit the characteristic mono-oxo V=O Raman vibration at 1038 cm^{-1} [39]. The same Raman band is also found for the supported $V_2O_5/Al_2O_3/SiO_2$ catalyst system under dehydrated conditions as well as supported V_2O_5/SiO_2 preventing discrimination of the coordination site of the surface VO_4 species [34]. However, titration of all the AlO_4 sites in ZSM-5 leads to crystalline V_2O_5 formation since the additional vanadium precursor has no sites to bind suggesting preferential coordination of the VO_4 units to the AlO_4 sites in ZSM-5. The preferential anchoring of the surface VO_4 sites to AlO_4 sites in ZSM-5 is confirmed by the enhanced specific rate of methanol oxidation for V_2O_5/ZSM-5 compared to V_2O_5/SiO_2 [39,40] as suggested by the reactivity findings for the supported V_2O_5/SiO_2 and V_2O_5/Al_2O_3 catalysts contained in Table 2.

3.2. Layered clays and hydrotalcites

Metal oxides, and especially vanadium oxide, have been successfully intercalated into layered metal hydroxides found in clays and hydrotalcites such as $Zn_2Al(OH)_6^+$ [33], $Zn_2Cr(OH)_6^+$ [41], $Ni_3Al(OH)_8^+$ [41], $Mg_2Al(OH)_6^+$ [41,42] and $Li_2Al(OH)_6^+$ [12]. Vanadium was ion exchanged into $Li_2Al(OH)_6^+$ layered hydroxide over the pH range of 3–11 [13]. Characterization studies showed that the vanadia in the interlayer was present as hydrated $V_2O_7^{4-}$ and $V_4O_{12}^{4-}$ species at room temperature. Heating to ~100 °C induced dimerization of $V_2O_7^{4-}$ to $V_4O_{12}^{4-}$ species in the interlayer, with further extent of polymerization upon heating to 350 °C. At higher temperatures the degradation of the layered framework took place with concomitant formation of crystalline Li_3VO_4 and $LiVO_3$. Intercalation of decavandate ($V_{10}O_{28}^{6-}$) into $Mg_2Al(OH)_6^+$ was also examined as a function of temperature [13]. At room temperature the intercalated decavanadate $V_{10}O_{28}^{6-}$ ion is present and begins to transform to simpler vanadate species (cyclic $(VO_3)_n^{n-}$ with n equal to 3 or 4, HVO_4^{2-} polymeric metavandates $(-O-VO_2-O-VO_2-O-)_n$ upon heating in the ~160–450 °C temperature range. The layered hydroxide structure is only stable until ~450 °C. At ~650 °C, the metavandate species react with the decomposed hydrotalcite to form the crystalline $Mg_2V_2O_7$ and $Mg(VO_4)_3$ bulk mixed oxides. The hydrated vanadate species observed in these layered hydroxides are similar to those found on hydrated oxide surfaces of simple oxides and their structures only depend on the net pH at point of zero charge (PZC) of the hydrated interlayer [43]. Although no catalytic data have been reported for the intercalated vanadium oxides in clays and hydrotalcites, it is important to point out that the interfacial vanadia species in clays and hydrotalcites are no different than the surface vanadia species observed for supported vanadium oxide catalysts. Thus, the catalytic properties of V-intercalated clays and hydrotalcites should be related to those reported for supported V_2O_5/Al_2O_3 and V_2O_5/MgO catalysts [1]. The major difference between the vanadate species intercalated into the hydroxide layers and more traditional supported metal oxides is that the former tend to thermally decompose at rather mild temperatures (~350 °C) in the presence of vanadium oxide,
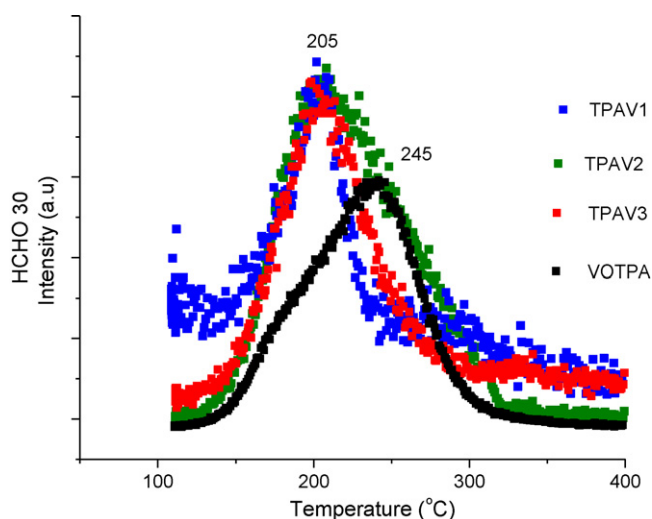
Fig. 2. HCHO/CH$_3$OH-TPSR spectra for V-containing tungstophosphoric acid catalysts.

which limits the use of clays and hydrotalcites as substrates for vanadium oxide at elevated temperatures.

3.3. Polyoxometalates (POMs)

V-containing POMs are usually prepared by substituting VO$_x$ units for WO$_x$ or MoO$_x$ units in the PW$_{12}$O$_{40}$ and PMo$_{12}$O$_{40}$ subnanometer Keggin structures, respectively [14]. The substituted VO$_x$ units take on distorted mono-oxo O=VO$_5$ coordination with four of the oxygen atoms bonded to adjacent W or Mo cations and the fifth oxygen atom weakly bonded to the central P heteroatom. Typically, only 1–3 VO$_x$ units are introduced into the Keggin structures since additional units will destabilize the POM [15]. It is generally assumed that all the VO$_6$ units have been substituted into the Keggin structure. The surface chemistry of a series of PW$_{12-x}$V$_x$O$_{40}$ Keggins was probed with CH$_3$OH-temperature programmed surface reaction (TPSR) spectroscopy and the findings are presented in Fig. 2. Without vanadia, the tungstophosphoric acid Keggin does not produce any HCHO because of the absence of surface redox sites in H$_3$PW$_{12}$O$_{40}$.

Substitution of one vanadia for a WO$_x$ site of tungstophosphoric acid, TPAV1, introduces redox sites that are reflected in the formation of the sharp HCHO peak at 205 °C. Substitution of two and three vanadia for WO$_x$ units of tungstophosphoric acid, TPAV2 and TPAV3, respectively, leads to broadening of the sharp HCHO/CH$_3$OH-TPSR band and introduction of a second redox site that forms HCHO at higher temperatures. The origin of the high temperature redox site was determined by impregnating a vanadium oxide precursor onto the tungstophosphoric acid Keggin, VOTPA, which results in formation of surface VO$_x$ species on the Keggin and the appearance of a broad HCHO/CH$_3$OH-TPSR peak

at 245 °C. The VOTPA TPSR experiment reveals that the broad HCHO/CH$_3$OH-TPSR features observed above 205 °C for TPAV2 and TPAV3 are a consequence of the presence of surface VO$_x$ species in addition to the vanadia sites substituted for WO$_x$ in TPA. Consequently, when more than one vanadia unit is substituted for a WO$_x$ site some of the vanadia is not incorporated into the Keggin structure.

The presence of the surface VO$_x$ species has significant catalytic consequences for the PW$_{12-x}$V$_x$O$_{40}$ Keggins. The much higher temperature for the formation of HCHO/CH$_3$OH-TPSR for the surface VO$_x$ species, 245 °C, relative to the substituted vanadia sites, 205 °C, demonstrates that the surface VO$_x$ species on the TPA Keggin are much less reactive than the VO$_x$ units incorporated into the Keggin structure. This is confirmed by the steady-state methanol oxidation TOF values and selectivity in Table 4 that show the specific redox activity of the V-containing TPA Keggin continuously decreases by orders of magnitude with increasing vanadia addition to PW$_{12-x}$V$_x$O$_{40}$ due to the increased surface VO$_x$ concentration on the TPA Keggin. Thus, the presence of surface VO$_x$ species on POM Keggins can significantly influence the catalytic features of V-containing Keggins.

3.4. Bulk mixed metal oxides

3.4.1. Bulk V$_2$O$_5$

Bulk V$_2$O$_5$ possesses an anisotropic morphology as depicted in Fig. 1 with the edge planes accounting for a minor fraction of the exposed surface area and the basal planes accounting for the majority of the exposed surface area. The basal planes terminate with V=O bonds and the edge planes possess V–OH and bridging V–O–V bonds. The surface chemistry of bulk V$_2$O$_5$ was chemical probed with CH$_3$OH chemisorption and methanol was found to selectively chemisorb on the edge planes. Consequently, the number of reactive exposed VO$_x$ sites for bulk V$_2$O$_5$ only corresponds to ~0.4 V/nm^2 [29,44] which is significantly less than the value of ~8 V/nm^2 typically found for supported vanadium oxide catalysts with monolayer surface VO$_x$ coverage (see Section 3.1 above on supported metal oxide catalysts).

The surface chemistry of bulk V$_2$O$_5$ was further chemically probed with CH$_3$OH-TPSR spectroscopy and found to exclusively produce HCHO as a reaction product reflecting the redox nature of the reactive surface VO$_x$ sites in bulk V$_2$O$_5$. The surface reactivity of bulk V$_2$O$_5$ was also examined with steady-state methanol oxidation at 230 °C and found to exhibit 90% HCHO selectivity and a TOF of ~4 × 10^{-1}/s. The high HCHO selectivity is a consequence of the redox nature of bulk V$_2$O$_5$ with the minor amount of acid sites responsible for 10% DME formation. Comparison of the TOF$_{redox}$ for bulk V$_2$O$_5$ with those for the supported vanadium oxide catalysts indicates that bulk V$_2$O$_5$ is rather reactive and is only surpassed by the supported V$_2$O$_5$/CeO$_2$ catalyst system.

The low reactivity of bulk V$_2$O$_5$ usually reported in the literature is then related to the low number of reactive surface VO$_x$ sites (~0.4 V/nm^2) because the basal planes are not active, and not to the true activity of the reactive surface VO$_x$ sites (~4 × 10^{-1}/s).

Table 4
Steady-state methanol oxidation over tungstophosphoric acid (TPA) and V-containing TPA (TPAV1, TPAV2, TPAV3 and VOTPA) polyoxometallates (6% CH$_3$OH, 13% O$_2$, 81% He; ~100 mL/min).

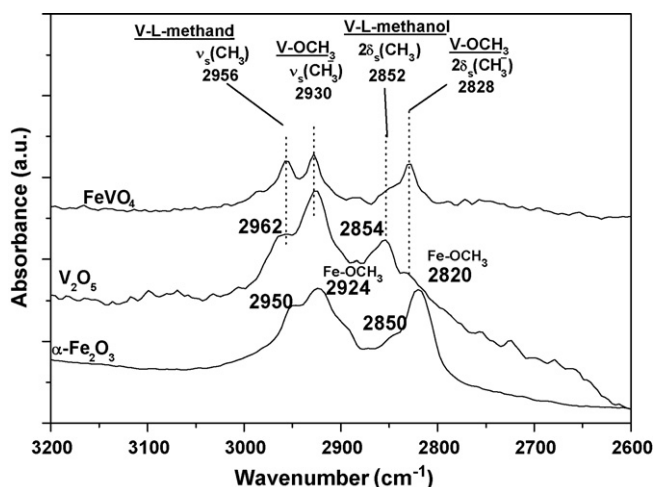| Catalyst	Temperature (°C)	Activity (mol/g cat s)	Selectivity		TOF (s^{-1})	
			DME	HCHO	Acid	Redox
TPA	225	9.6	100	0	3.9	0.0
TPAV1	225	14.7	82	18	7.6	0.32
TPAV2	225	7.4	90	10	0.46	0.01
TPAV3	225	3.0	100	0	1.9	0.00
VOTPA	250	12.5	88	12	0.12	0.0054
VOTPA	225 (extrapolated)	–	–		0.46	0.0021

Fig. 3. CH_3OH-IR spectra for Fe_2O_3, V_2O_5 and $FeVO_4$ (L refers to intact CH_3OH coordinated to surface Lewis acid sites).

Fig. 4. HCHO and DME products obtained during the CH_3OH-TPSR from Fe_2O_3, V_2O_5 and $FeVO_4$ catalysts.

Furthermore, this fact also reveals that the enhanced activity of supported V_2O_5 catalysts is mostly related to the high number of reactive surface VO_x sites ($\sim$8 V/nm^2) at monolayer coverage.

3.4.2. Bulk metal vanadates

V-containing bulk mixed metal oxides are traditionally synthesized by wet coprecipitation methods followed by calcination at elevated temperatures [5], but can also be formed via solid-state reactions [16]. The V-containing bulk mixed metal oxides are crystalline and typically possess low BET surface area, $\sim$1–20 m^2/g. The coordination of VO_x in bulk mixed metal oxides varies from VO_4, VO_5 to VO_6, with VO_6 being somewhat more prevalent [45]. Bulk $FeVO_4$ consists of three distinct, isolated VO_4 units that are distorted and are each coordinated to four FeO_6 units [46]. The Raman spectrum of bulk $FeVO_4$ exhibits three bands at 971, 936 and 910 cm^{-1} representing the shortest V=O bonds of the each of the three distinct VO_4 sites, respectively [5]. Chemisorption of CH_3OH on bulk $FeVO_4$ only exhibits IR vibrations of surface CH_3O^* intermediates, $\sim$2820–2830 and 2920–2930 cm^{-1}, and intact chemisorbed surface CH_3OH^* species, $\sim$2850–2860 and $\sim$2950–2960 cm^{-1}, on surface Lewis acid sites as shown in Fig. 3. For comparison, the M–OCH_3 vibrations for Fe–OCH_3 on bulk Fe_2O_3 occur at 2820 and 2924 cm^{-1} and are shifted to 2828 and 2930 cm^{-1} for V–OCH_3 on bulk V_2O_5. The M–OCH_3 vibrations on bulk $FeVO_4$ line up with the vibrations of V–OCH_3 and there is no evidence of significant Fe–OCH_3 IR bands. The absence of surface Fe–OCH_3 vibrations reveals that the surface CH_3O^* intermediate preferentially bonds to surface VO_x sites and suggests that surface of bulk $FeVO_4$ is significantly enriched with surface VO_x sites.

The surface chemistry of bulk Fe_2O_3, V_2O_5 and $FeVO_4$ was chemically probed with CH_3OH-TPSR spectroscopy as shown in Fig. 4. The bulk Fe_2O_3 catalyst primarily yields dimethyl ether (DME:CH_3OCH_3) from surface acid sites and a minor amount of HCHO from surface redox sites [44,47]. In contrast, bulk V_2O_5 almost exclusively produces HCHO because of the dominance of surface redox sites in this material [5,48]. Bulk $FeVO_4$ also only gives rise to HCHO reflecting the predominance of surface redox sites on its surface, which are the surface VO_x species that are enriched on the surface of bulk $FeVO_4$. This conclusion is further confirmed by steady-state methanol oxidation over the bulk Fe_2O_3, V_2O_5 and $FeVO_4$ presented in Table 5. Bulk Fe_2O_3 does not form any HCHO reflecting the low concentration of surface redox sites and primarily produces DME and dimethoxy methane (DMM:$(CH_3O)_2CH_2$). Formation of DMM requires the presence of surface redox that give HCHO and surface acid sites that subsequently couple HCHO with

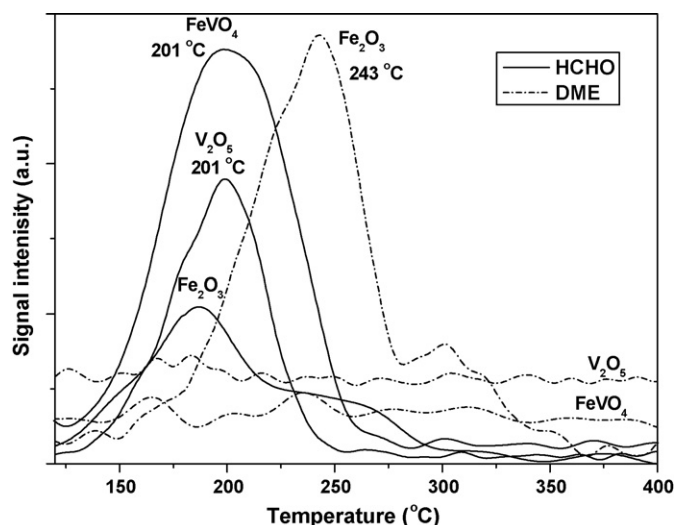two surface CH_3O^* intermediates [48]. The predominance of DME on Fe_2O_3 is a consequence of the dominance of acid sites on its surface. In contrast, bulk V_2O_5 primarily gives rise to HCHO reflecting the dominance of redox sites on its surface and only gives rise to a minor amount of DMM without the formation of any DME. The bulk $FeVO_4$ catalyst, however, behaves very similar to the bulk V_2O_5 catalyst with its surface redox sites and exhibits almost the same product selectivity and TOF value. Consequently, the catalytic properties of bulk $FeVO_4$ do not reflect the characteristics of acidic FeO_x sites and are completely overwhelmed by the redox properties of the surface redox VO_x sites.

The conclusion that a surface enriched VO_x outer layer is present for the bulk $FeVO_4$ phase is further supported by steady-state methanol oxidation over a supported 4% V_2O_5/Fe_2O_3 catalyst that contains about monolayer coverage of surface VO_x species on the Fe_2O_3 support [5]. Methanol oxidation over the supported V_2O_5/Fe_2O_3 catalyst leads to a very high HCHO selectivity reflecting the dominance of redox surface VO_x sites, whereas, bulk Fe_2O_3 yields significant amounts of DME from its surface acid sites.

3.4.3. Bulk mixed oxide solid solutions

Bulk mixed oxide solid solutions of vanadium oxide with other oxides are well known (e.g., $V_xTi_{1-x}O_2$ (rutile) and $V_xNb_{2-x}O_5$ [17]). Such catalytic materials are inherently inactive since the redox VO_x sites are incorporated inside the mixed metal oxide structure and, consequently, are not accessible to the reactant molecules at its surface. For example, the bulk mixed oxide $V_xTi_{1-x}O_2$ (rutile) solid solution phase is essentially inactive and unselective for o-xylene oxidation to phthalic anhydride, but its catalytic performance is significantly improved once additional vanadium oxide is impregnated onto its surface [17]. In the case of $V_xNb_{2-x}O_5$ solid solutions, Raman spectroscopy reveals that dehydrated surface VO_x species are present on the surface of $V_xNb_{2-x}O_5$ [49]. By comparing the

Table 5
Steady-state methanol oxidation over bulk Fe_2O_3, V_2O_5 and $FeVO_4$ catalysts at 230 °C (6% CH_3OH, 13% O_2, 81% He; $\sim$100 mL/min).

Catalyst	TOF (s^{-1})	Selectivity		
		HCHO	DME	DMM
Fe_2O_3	–	0	70	30
V_2O_5	0.4	87	0	13
$FeVO_4$	0.16	83	0	17

Table 6
Catalytic properties of bulk $V_xNb_{2-x}O_5$ mixed metal oxides for propane oxidative dehydrogenation reaction at $400\,^\circ C$(5% C_3H_8, 40% O_2, 55% He; ~50 mL/min; C_3 conversion <5%).

Catalysts	Selectivity to C_3H_6	Fraction of VO_x on surface	TOF ($10^{-3}\,s^{-1}$)
Nb_2O_5	100	0.0	0.1[a]
1% V–Nb–O	100	0.34	4.8[b]
5% V–Nb–O	64.5	0.34	3.6[b]
10% V–Nb–O	67.6	0.57	3.6[b]

[a] Number of active surface niobia sites on pure Nb_2O_5 determined by 2-propanol chemisorption.
[b] Number of surface VO_x sites estimated by comparison with supported V_2O_5/Nb_2O_5 catalysts [47].

catalytic activity of the mixed $V_xNb_{2-x}O_5$ solid solution with that of supported V_2O_5/Nb_2O_5 containing a monolayer of surface VO_x species for oxidative dehydrogenation (ODH) of propane to propylene, which requires only one surface VO_x site to proceed, it was possible to estimate the fraction of VO_x that is present on the surface and bulk of the mixed $V_xNb_{2-x}O_5$ solid solution since NbO_x sites are essentially inactive for this ODH reaction. The distribution of VO_x between the bulk and surface of $V_xNb_{2-x}O_5$ as well as the corresponding catalytic data are listed in Table 6.

The propane ODH studies over the bulk $V_xNb_{2-x}O_5$ mixed oxide solution reveal that the activity of this catalytic reaction is significantly enhanced when surface VO_x sites are present on $V_xNb_{2-x}O_5$ solid solution, which are the catalytic active sites. Furthermore, the data show that a significant fraction of the VO_x that has been introduced into the mixed $V_xNb_{2-x}O_5$ solid solution is always on the surface of this mixed oxide solid solution. Thus, surface VO_x species are always present on the surfaces of mixed oxide solid solutions and are the active sites that control their catalytic properties.

4. Conclusions

V-containing mixed oxides (supported metal oxides, zeolites and molecular sieves, layered clays and hydrotalcites, polyoxometalates (POMs), bulk mixed oxides and mixed oxide solid solutions) were investigated for the presence of surface VO_x phases and their influence on catalytic reactions. Supported VO_x catalysts on traditional oxide supports were used as model systems to better understand the structure and property of surface VO_x species since they are 100% dispersed on the high surface area oxide supports below monolayer coverage. Surface VO_x species were found to be present on all types of V-containing mixed oxides (zeolites and molecular sieves, layered clays and hydrotalcites, polyoxo metallates (POMs), bulk mixed oxides and mixed oxide solid solutions). Furthermore, the surface VO_x species were found to be the catalytic active sites for all types of the V-containing mixed oxides. These findings reveal the generality of surface vanadium oxide phases in V-containing mixed oxide catalytic materials. Furthermore, surface MO_x phases are generally also present for other mixed oxide system containing low Tammann temperature oxides (e.g., MoO_3, CrO_3, WO_3 and Re_2O_7).

References

[1] G. Deo, I.E. Wachs, J. Catal. 129 (1991) 307–312.
[2] G. Deo, I.E. Wachs, J. Catal. 146 (1994) 323–334.
[3] J. Haber, T. Machej, E.M. Serwicka, I.E. Wachs, Catal. Lett. 32 (1995) 101–114.
[4] C.-B. Wang, Y. Cai, I.E. Wachs, Langmuir 15 (1999) 1223–1235.
[5] L.E. Briand, J.-M. Jehng, L. Cornaglia, A.M. Hirt, I.E. Wachs, Catal. Today 78 (2003) 257–268.
[6] N. Das, H. Eckert, H. Hu, I.E. Wachs, J.F. Walzer, F.J. Feher, J. Phys. Chem. 97 (1993) 8240–8243.
[7] X. Gao, S.R. Bare, B.M. Weckhuysen, I.E. Wachs, J. Phys. Chem. 102 (1998) 10842–10852.
[8] E.L. Lee, I.E. Wachs, J. Phys. Chem. C 111 (2007) 14410–14425.
[9] J.L. Bronkema, D.C. Leo, A.T. Bell, J. Phys. Chem. C 111 (2007) 14530–14540.
[10] H. Tian, E.I. Ross, I.E. Wachs, J. Phys. Chem. B 110 (2006) 9593–9600.
[11] X. Gao, I.E. Wachs, J. Phys. Chem. B 104 (2000) 1261–1268.
[12] J. Twu, P.K. Dutta, J. Phys. Chem. 93 (1989) 7863–7868.
[13] J. Twu, P.K. Dutta, J. Catal. 124 (1990) 503–510.
[14] R.S. Weber, J. Phys. Chem. 98 (1994) 2999–3005.
[15] D. Casarini, G. Centi, P. Jiru, V. Lena, Z. Tvaruzkova, J. Catal. 143 (1993) 325–344.
[16] I.E. Wachs, L.E. Briand, US Patent 7,193,117, B2, 2007.
[17] R.Y. Saleh, I.E. Wachs, S.S. Chan, C.C. Chersich, J. Catal. 98 (1986) 102–114.
[18] T. Kim, I.E. Wachs, J. Catal. 255 (2008) 197–205.
[19] I.E. Wachs, L.E. Briand, Int. Patent. WO 03/053556, A2, 2003.
[20] C. Zhao, I.E. Wachs, J. Catal. 257 (2008) 181–189.
[21] Y. Chen, I.E. Wachs, J. Catal. 217 (2003) 468–477.
[22] B. Kilos, A.T. Bell, E. Iglesia, J. Phys. Chem. C 113 (2009) 2830–2836.
[23] J.P. Dunn, P.R. Koppula, H.G. Stenger, I.E. Wachs, Appl. Catal. B: Environ. 19 (1998) 103–117.
[24] X. Gao, M.A. Banares, I.E. Wachs, J. Catal. 188 (1999) 325–331.
[25] M.D. Argyle, K. Chen, A.T. Bell, E. Iglesia, J. Catal. 208 (2002) 139–149.
[26] X. Gao, J.-M. Jehng, I.E. Wachs, J. Catal. 209 (2002) 43–50.
[27] I.E. Wachs, J.-M. Jehng, G. Deo, B.M. Weckhusyen, V.V. Guliants, J.B. Benziger, S. Sundaresan, J. Catal. 170 (1997) 75–88.
[28] I.E. Wachs, G. Deo, B.M. Weckhusyen, A. Andreini, M.A. Vuurman, M. De Boer, M.D. Amiridis, J. Catal. 161 (1996) 211–221.
[29] I.E. Wachs, Y. Chen, J.-M. Jehng, L.E. Briand, T. Tanaka, Catal. Today 78 (2003) 13–24.
[30] A. Goodrow, A.T. Bell, J. Phys. Chem. C 112 (2008) 13204–13214.
[31] X. Gao, S.R. Bare, J.L.G. Fierro, M.A. Banares, I.E. Wachs, J. Phys. Chem. B 102 (1998) 5653–5666.
[32] X. Gao, J.L.G. Fierro, I.E. Wachs, Langmuir 15 (1999) 3169–3178.
[33] X. Gao, I.E. Wachs, J. Catal. 192 (2000) 18–28.
[34] E.L. Lee, I.E. Wachs, J. Phys. Chem. C 112 (2008) 20418–20428.
[35] E.I. Ross-Medgaarden, I.E. Wachs, W.V. Knowles, A. Burrows, C.J. Kiely, M.S. Wong, J. Am. Chem. Soc. 131 (2009) 680–687.
[36] X. Gao, S.R. Bare, J.L.G. Fierro, I.E. Wachs, J. Phys. Chem. B 103 (1999) 618–629.
[37] H. Knozinger, E. Taglauer, Catalysis 10 (1993) 1–40.
[38] C.-B. Wang, G. Deo, I.E. Wachs, J. Catal. 178 (1998) 640–648.
[39] E.L. Lee, I.E. Wachs, in: I. Halsaz (Ed.), Silica and Silicates in Modern Catalysis, Transworld Research Network, Kerala, India, 2010, pp. 1–32.
[40] E.L. Lee, I.E. Wachs, J. Catal. 258 (2008) 103–110.
[41] T. Kwon, G.A. Tsigdinos, T.J. Pinnavaia, J. Am. Chem. Soc. 110 (1988) 3653–3654.
[42] M.A. Drezdzon, Inorg. Chem. 27 (1988) 4628–4632.
[43] G. Deo, I.E. Wachs, J. Phys. Chem. 95 (1991) 5031–5041.
[44] M. Badlani, I.E. Wachs, Catal. Lett. 75 (2001) 137–149.
[45] A.F. Wells, Structural Inorganic Chemistry, 5th ed., Oxford University Press, NJ, 1983.
[46] M. Kurzawa, E. Tomaszewicz, Spectrochim. Acta A 55 (1999) 2889–2892.
[47] J.M. Tatibouët, Appl. Catal. A 148 (1997) 213–252.
[48] J.M. Tatibouët, H. Lauron-Pernot, J. Mol. Catal. A: Chem. 171 (2001) 205–216.
[49] Z. Zhao, X. Gao, I.E. Wachs, J. Phys. Chem. B 107 (2003) 6333–6342.